Cyclin-Like Proteins Tip Regenerative Balance in the Liver to Favour Cancer Formation

Author List: Bre-Anne Fifield[1], John Talia[1], Carlee Stoyanovich[1], Mitchell J. Elliott[1], Martin K. Bakht[1], Amy Basilious[1], Joshua P. Samsoondar[1], Madison Curtis[1], Keith F. Stringer[1, 2], Lisa A. Porter[1]*

[1]Department of Biological Sciences
University of Windsor
Windsor, ON N9B 3P4

[2]Department of Pathology
Cincinnati Children's Hospital Medical Center
Cincinnati, United States

*Corresponding Author

fifield@uwindsor.ca
taliaj@uwindsor.ca
carlee.stoyanovich@mail.utoronto.ca
mitchell.elliott@mail.utoronto.ca
khosra11@uwindsor.ca
basilioa@uwindsor.ca
jsamsoon@uwo.ca
curti115@uwindsor.ca
stringek@uwindsor.ca
lporter@uwindsor.ca

Keywords: Cdk, Cyclin, cell cycle, hepatocellular carcinoma, regeneration, liver, fibrosis

Financial Support: B.F. acknowledges scholarship support from the University of Windsor, the Ontario Graduate Scholarship Program and the Canadian Breast Cancer Foundation. This work was supported by a Windsor Cancer Centre Foundation Seeds4Hope grant and a Canadian Institutes Health Research grant to L.A.P (Grant#142189).

Conflict of Interest: The authors have no conflicts to disclose.

Abstract

Hepatocellular carcinoma (HCC) is one of the leading causes of cancer related deaths world-wide. A variety of factors can contribute to the onset of this disease, including viral infection, obesity, alcohol abuse and non-alcoholic fatty liver disease (NAFLD). These stressors predominantly introduce chronic inflammation leading to liver cirrhosis and finally the onset of HCC, however approximately 20% of HCC cases arise in the absence of cirrhosis via a poorly defined mechanism. The atypical cyclin-like protein Spy1 is capable of overriding cell cycle checkpoints, promoting proliferation and has been implicated in HCC. We hypothesize that Spy1 promotes sustained proliferation making the liver more susceptible to accumulation of deleterious mutations and leading to the development of non-cirrhotic HCC. We report for the first time that elevation of Spy1 within the liver of a transgenic mouse model leads to enhanced spontaneous liver tumourigenesis. We show that the abundance of Spy1 enhanced fat deposition within the liver and decreased the inflammatory response. Interestingly, Spy1 transgenic mice have a significant reduction in fibrosis and sustained rates of hepatocyte proliferation, and endogenous levels of Spy1 are downregulated during the normal fibrotic response. Our results provide support that abnormal regulation of Spy1 protein drives liver tumorigenesis in the absence of elevated fibrosis and hence may represent a potential mechanism behind non-cirrhotic HCC. This work may implicate Spy1 as a prognostic indicator and/or potential target in the treatment of diseases of the liver, such as HCC.

Introduction

Hepatocellular carcinoma, HCC, is one of the leading causes of cancer related death worldwide, with a five year survival rate of only 20% (1). Prognosis is poor, mainly due to the limited treatment options and the central role the liver plays in basic human functions such as detoxification and cholesterol metabolism. Prevalence of HCC in developing and developed nations can be attributed to a variety of factors including hepatitis B or C infection, and exposure to aflatoxins, or diabetes, chronic alcoholism and cirrhosis of the liver (2-4). Cirrhosis of the liver can be triggered by long term alcohol abuse triggering accumulation of lipid droplets within the liver leading to increased inflammation and fibrosis (5). Cirrhosis can also occur independent of alcoholism, including the progression of non-alcoholic fatty liver disease (NAFLD) to non-alcoholic steatohepatitis (NASH), events which precipitate often as a result of obesity (6). While cirrhosis is known to be a major driver for development of HCC, approximately 20% of all cases form in the absence of cirrhosis (7). NAFLD is a known risk factor for HCC and incidence is on the rise, with approximately one-third of adults affected in the Western world, likely due to increasing rates of obesity, and metabolic syndromes such as diabetes (8). HCC arising from NAFLD can also occur without evidence of advanced fibrosis (9). Thus, it is of high importance to understand the molecular mechanisms mediating the onset and initiation of HCC in the non-cirrhotic liver in the presence of NAFLD.

NAFLD is characterized by increased fat accumulation in the liver (6). In and of itself, this condition is not typically harmful and symptoms may be absent. Changes in diet, and increased weight loss can help to reverse NAFLD (6,10). Fat accumulation in the liver becomes more dangerous when it begins to trigger inflammatory response pathways leading to injury and cellular damage (6,10). As a protective response, the master regulator and tumour suppressor p53 is triggered and transcribes cell cycle inhibitors like $p21^{CIP1}$ (11,12). Fatty liver diseases have increased levels of p53, $p21^{CIP1}$and decreased levels of anti-apoptotic proteins such as Bcl-XL (13-15). Tumour suppressors such as PTEN and p53 may accelerate the development of steatosis,

thereby aiding in the induction of cellular damage within the setting of NAFLD (9,15,16). The accumulation of fat within the liver can therefore create an environment characterized by increased cellular damage and injury, an environment primed for development of HCC.

In normal circumstances, injured or lost hepatocytes possess a remarkable capacity for regeneration, where the quiescent hepatocyte population is primed to respond to mitogenic signals to stimulate re-entry into the cell cycle (17-19). Hepatocytes undergo multiple rounds of highly synchronized DNA replication and division to reconstitute the injured area or to compensate for lost tissue (17,18). In models of partial hepatectomy, the liver is capable of sustaining loss of two-thirds of the overall tissue mass and can regenerate this mass within a week demonstrating the remarkable proliferative capacity of hepatocytes (18,20,21). During the regenerative process, there is also a transient increase in fat accumulation coinciding with waves of hepatocyte proliferation (22). It has been proposed that this transient increase in fat during regeneration is to meet the increased energy demands of rapidly proliferating hepatocytes (22). In accordance with this hypothesis, it is known that cancer cells often have increased lipid droplet accumulation (23).

Over time, the level of damage sustained by the hepatocytes exceeds their capacity to proliferate (6). When the ability to regenerate damaged areas is lost, injury is sustained and the liver begins to activate apoptotic pathways to remove injured and damaged hepatocytes from the population. Increased hepatocyte apoptosis is crucial for the removal of potentially deleterious mutations from the population, and is often seen in cases of NAFLD (24). Inactivation of checkpoints and inhibition of pro-apoptotic pathways allows for continual proliferation of damaged cells leading to carcinogenesis. This can occur concomitant with a loss of heterozygosity of tumour suppressors and a decrease in ploidy (25).

DNA damage response (DDR) pathways and cell cycle regulation both play a critical role in hepatocyte proliferation in response to injury and inflammation. The cyclin-like protein Spy1 is capable of binding and activating Cyclin Dependent Kinase 2 (CDK2) in the absence of canonical phosphorylation, leading to increased CDK2 activity and enhanced progression through the cell

cycle (26-29). Spy1 was initially isolated in a screen for genes that can override DDR checkpoints and further study has demonstrated that this cell cycle mediator promotes cell cycle progression in the presence of damage and overrides apoptosis in a p53-dependent manner (30,31). Thus, Spy1 plays a critical role in regulating cell cycle progression and response to damage. Previous reports have found Spy1 levels to be high in human HCC when compared to pair matched normal tissue, and increasing levels correlated with increasing severity of disease and poor prognosis (32). Levels of Spy1 also correlated positively with the proliferation marker Ki67, highlighting the importance of this protein in promoting cell cycle progression (32). Collectively, Spy1 may play a critical role in tumour initiation and progression in the liver.

Herein we describe a surprising phenotype in male mice containing a Spy1 transgene driven by an MMTV promoter. These mice develop tumours in the liver at a significantly higher rate than their control littermates. Histological analysis revealed the presence of increased fat accumulation in livers of male MMTV-Spy1 mice in addition to a decrease in the deposition of fibrous material. We describe a potential role for Spy1 in increasing liver cancer susceptibility in the non-cirrhotic liver by keeping the liver in a more proliferative state thereby promoting the development of non-cirrhotic HCC. Hence, elevated Spy1 levels favour continued cellular proliferation in the presence of damage, thereby increasing susceptibility to tumourigenesis.

Materials and Methods

Maintenance of MMTV-Spy1 Transgenic Mice

MMTV-Spy1 (B6CBAF1/J-Tg(MMTV-Spy1)1Lport) mice were generated and maintained as described (33). Mice were maintained on a 12 hour light dark cycle with ad libitum access to water, and were fed standard rodent laboratory chow (Purina 5001) unless otherwise indicated. Mice were maintained following the Canadian Council on Animal Care Guidelines under the animal utilization protocol #14-22 approved by the University of Windsor.

Methionine-Choline Deficient (MCD) Diet

MCD and amino acid control diet (Harlan) was administered ad libitum beginning at 8 to 12 weeks of age for B6CBAF1/J and over 1 year of age for MMTV-Spy1 and control littermates.

Plasmids

The pCS3 and Myc-Spy1 pCS3 plasmids were used in overexpression experiments and were generated as previously described (27,34). For knockdown experiments, pLKO.1 (Addgene) and pLKO.shSpy1.2 were generated and used as described (27). The pEIZ plasmid was a kind gift from Dr B. Welm, and the pEIZ-Flag-Spy1 vector was generated as previously described (34).

Cell Culture and Transfection

HepG2 cells (a kind gift from Dr. Hudson, University of Windsor) were maintained in Eagle's Minimum Essential Medium (EMEM) supplemented with 10% FBS and 1% penicillin/streptomycin at 37°C, 5% CO_2. THLE-2 cells were purchased from and authenticated by ATCC (CRL 2706) and were maintained using the BEGM Bullet Kit (CC3170) at 37°C, 5% CO_2. HepG2 cells were transfected using polyethylenime (PEI) branched reagent (Sigma). Briefly, 40µg of PEI and 10µg of plasmid were incubated together for 10 minutes before adding to a 10cm plate. THLE-2 cells were transfected using polyethylenime (PEI) branched reagent (Sigma). Briefly, 10µg of PEI and 6µg of plasmid were incubated together for 10 minutes before adding to a 6cm plate. Cells were subject to routine mycoplasma testing.

Histology and Immunostaining

Tissue was collected and fixed in 10% neutral buffered formalin for paraffin embedding, and 4% paraformaldehyde for frozen sectioning. Immunohistochemistry was performed as described (35). Primary antibodies used were as follows: p53 (1:200; Abcam; ab131442), p21 (1:200; Abcam; ab109199), Cleaved Caspase-3 (1:200; Cell Signaling; 9661), BrdU (1:200; BD Biosciences; 555627), PCNA (1:500; Santa Cruz; sc-9857), CD10 (1:200; Novus; NBP2-15771); α-smooth

muscle actin (Novus; NBP2-21748); F4/80 (Thermo; 14-4801-82). Mouse on Mouse (MOM) blocker (Biocare Medical) or 3% BSA-0.1% Tween-20 in 1x PBS was used for mouse and rabbit or goat secondary antibodies respectively. Secondary antibody (Vector Laboratory) was used at a concentration of 1:750. Sections were subsequently incubated with ABC reagent as per manufacturer's instructions (Vectastain ABC Kit). Sections were visualized using the LEICA DMI6000 inverted microscope with LAS 3.6 software. The integrated density of the stain was quantified using ImageJ software and corrected for using the integrated density of the nuclear control. Pathology assessments were confirmed by board certified pathologist Dr. K.F. Stringer (author on publication) and Dr. Robert Cardiff.

Primary Hepatocyte Isolation and Flow Cytometry Analysis

Primary hepatocytes were isolated from MMTV-Spy1 mice and their control littermates over a year of age using the collagenase perfusion method as described (36). Isolated hepatocytes were stained with propidium iodine to assess DNA content using the BD LSR Fortessa™ X- 20.

Xenograft Transplantation

HepG2 cells were transfected with pEIZ, pEIZ-Spy1, pLKO or pLKO-shSpy1 and $5x10^6$ manipulated cells were injected subcutaneously into the flanks of male Nu/Nu mice (Charles River; 088). Tumour volume was monitored and measured twice weekly using calipers.

Statistical Analysis

For statistical analysis of tumour studies, a Mann-Whitney test was performed. A Student's T-Test was performed for all other data. Unequal variance was assumed for experiments involving mouse tissue samples and primary cells. Cell line data analysis assumed equal variance. All experiments, including animal studies, included at least 3 biological replicates, and results are representative of at least three experiments. No randomization or blinding occurred for animal studies. Significance was scored as *p<0.05, **p<0.01, ***p<0.001.

Additional Materials and Methods can be found in S1 Supplemental Materials and Methods File

Results

Male MMTV-Spy1 exhibit an increase in Spy1 and increased tumourigenesis.

MMTV-Spy1 mice were generated on a B6CBAF1/J background to study the effects of increased Spy1 protein levels on mammary development and tumourigenesis as part of a separate study and full examination of transgene expression levels was conducted (33). Given that the MMTV promoter can show residual activity in other tissue types in a gender-specific manner, non-productive MMTV-Spy1 male breeders and their control littermates were sacrificed once they reached one year of age to assess transgene expression (37). Upon sacrifice, it was noted that MMTV-Spy1 males over one year of age displayed a significant increase in liver tumour formation as compared to control littermates of the same age (Figure 1A). No liver tumours were noted in any aged female control or MMTV-Spy1 mice. Tumours were confirmed to be primary liver tumours by 2 independent board-certified pathologists. The addition of CD10 immunohistochemistry and whole-body necropsy were also performed to ensure that these were primary liver tumours (Figure S1A). Liver tissue was extracted from aged males and *SPDYA* expression levels were found to be significantly increased in liver tissue from MMTV-Spy1 males at both the mRNA and protein level, but not in other tested tissues (Figure 1B, S1B, S1C-D). When levels of Spy1 were examined in aged female mice, the same trend was not noted (Figure S1E), indicating that expression of Spy1 and tumour onset is specific to male MMTV-Spy1 mice.

Elevated levels of Spy1 lead to increased fat accumulation.

NAFLD and NASH can be characterized by increased lipid accumulation within the liver which ultimately leads to increased inflammation and fibrosis, contributing to the development of HCC

(5,6). To determine if elevated levels of Spy1 leads to morphological changes in the liver of aged mice, liver tissue was collected, fixed and stained to assess the pathology of the livers (Figure 1C). Gross morphological changes were noted in the livers of MMTV-Spy1 male mice, particularly the presence of large vacuoles which could be indicative of fat deposition within the liver. Oil-Red-O staining was performed to determine if these large vacuoles were indeed fatty deposits in the liver (Figure 1D). MMTV-Spy1 male mice had significantly more fat than their control littermates, whereas female mice showed no differences in morphology or fat accumulation (Figures S1F-G). To validate these findings, liver triglyceride content was assessed and was found to be significantly increased in MMTV-Spy1 mice, consistent with the histological findings (Figure 1E). To determine the direct effects of increased Spy1 levels on fat accumulation, we utilized the well characterized THLE-2, normal hepatocyte cell line and HepG2 HCC cell line. Using these cells, we overexpressed Spy1 (Figure S2A) and examined the effects of elevated Spy1 on accumulation of fat within hepatocytes. Using Oil Red O staining, we show that overexpression of Spy1 increases lipid accumulation in THLE-2 and HepG2 cells (Figure S2B). In contrast, knockdown of Spy1 (Figure S2C) leads to a significant decline in Oil Red O staining (Figure S2D). To determine if Spy1 directly affected de novo lipogenesis, expression of a panel of lipogenic proteins was assessed via qRT-PCR in control and MMTV-Spy1 mice as well as HepG2 cells with elevated Spy1. Levels of Cpt1a and Srebf2 were found to be significantly decreased in MMTV-Spy1 mice as compared to littermate controls, and overexpression of Spy1 in HepG2 cells resulted in significant decreases in not only Cpt1a and Srebf2, but also Acox (Figure S3). Collectively these data support the conclusion that elevated levels of Spy1 correlate with lipid accumulation in the liver and lead to decreased fatty acid catabolism, a hallmark of NAFLD and NASH.

Elevated levels of Spy1 increase markers of DDR and decrease protective apoptotic and fibrotic responses.

Fatty liver diseases such as NASH can lead to up-regulation of inflammatory and DDR pathways in response to increased damage and injury the liver sustains due to increased fat accumulation (6). Levels of the tumour suppressor p53 are increased in cases of NASH, positively correlating with the degree of inflammation (14,15). Given that Spy1 is known to override the DDR, specifically the effects of p53, we questioned whether there were alterations in p53 signaling in the MMTV-Spy1 mice (33). Analysis of p53 levels via immunohistochemistry revealed a significant increase in the levels of p53 protein in MMTV-Spy1 male livers as compared to control (Figure 2A). Levels of p21, a known downstream target of p53, are also increased in MMTV-Spy1 livers (Figure 2B), supporting the hypothesis that there is accumulating damage in the MMTV-Spy1 livers. Triggering of apoptosis to remove severely damaged cells is an important protective response in cases of NAFLD/NASH (14). Through immunohistochemistry, we find a decrease in the levels of cleaved-caspase 3, a central player in the apoptotic pathway commonly used to indicate increased amounts of apoptosis (Figure 2C). Levels of albumin and p27, both known to play important roles in NASH were also examined and show no statistically significant differences (Figure S4A-C). Another hallmark of NASH is increased expression of TNFa, an inflammatory response marker upregulated during the onset of fibrosis (38,39). Fibrotic tissue provides structural protection to the organ when copious amounts of damage can no longer be repaired via hepatocyte proliferation(5,40). MMTV-Spy1 mice have a significant decrease in TNFa (Figure 2D) and less fibrosis than their littermate controls (Figure 2E). Non-parenchymal cells of the liver, Kupffer and stellate cells, both play crucial roles in the fibrotic and inflammatory response (41,42). Kupffer cells, which can be detected via expression of F4/80, are a major source of TNFa and driver of stellate cell activation, detected through increased expression of α-smooth muscle actin (42,43). Changes in Kupffer and stellate cell populations were assessed via immunohistochemistry. MMTV-Spy1 were found to have significantly less

Kupffer cells, correlating with decreased TNFa (Figure 2F). There was no significant difference seen in stellate cell activation despite decreased fibrosis, as indicted by no change in smooth muscle actin (Figure S4D). Thus, MMTV-Spy1 male mice demonstrate increased DDR signaling consistent with elevated damage occurring due to fat accumulation. However, MMTV-Spy1 livers have decreased protection from apoptotic and fibrotic responses.

Elevated Spy1 leads to increased proliferative capacity of hepatocytes.

The proliferative capacity of the hepatocytes was assessed to determine if this could be a contributing factor to the development of HCC. Hepatocytes are relatively quiescent cells and frequently exhibit bi-nucleated cells and increased polyploidy (44). As the liver progresses to a more proliferative state and advances to HCC, data suggests that the number of bi-nucleated cells and DNA content declines (45). The percentage of bi-nucleated cells was determined in the MMTV-Spy1 and littermate control mice and the data reveals that Spy1 overexpression results in a reduction in the number of bi-nucleated cells (Figure 3A). To determine if the decrease in bi-nucleated cells also indicated a reduction in DNA content, primary hepatocytes were isolated from MMTV-Spy1 mice and their control littermates and assessed via flow cytometry. MMTV-Spy1 displayed a significant increase in cells with 2N DNA content as well as a significant reduction in tetraploid cells potentially indicating enhanced proliferation (Figure 3B). To further confirm this finding, MMTV-Spy1 mice and their control littermates were injected with BrdU and the percentage of BrdU positive cells was assessed. MMTV-Spy1 mice had a significant increase in the percentage of BrdU positive cells (1.45%) over their control littermates (0.61%) (Figure 3C). It is notable that MMTV-Spy1 cells appear smaller than control cells, while not quantified, this observation could be consistent with the increase in proliferation and a decrease in binucleation. PCNA staining was also used to support this finding and MMTV-Spy1 mice were found to have a significant increase in the percentage of PCNA positive cells (Figure 3D). Mechanistically we have found that while Cyclin D protein levels decline with age, this was not a significantly changed between control and MMTV-Spy1 mice at any age (Figure S5C-D). The

cell cycle inhibitor p21 was significantly upregulated in MMTV-Spy1 mice during aging, further validating our previous finding (Figure 2B). Expression of the cyclins were also assessed in HepG2 cells with Spy1 overexpression and no changes were noted (Figure S5F).

Hepatocytes are normally held in a state of quiescence in part through C/EBPa inhibition of the cell cycle (46). Interestingly, C/EBPa levels were significantly decreased in MMTV-Spy1 mice as compared to littermate controls in both young and aged mice (Figure S5E). Proliferation was further validated by BrdU incorporation assays in HepG2 and THLE-2 cells with Spy1 overexpression or knockdown, where the number of BrdU positive cells was significantly increased or decreased respectively (Figure S5A-B). Taken together this data suggests that Spy1 is enhancing the proliferative potential of the liver and that this may be due to a reduction in the transcription factor C/EBPa.

Spy1 decreases with the onset of fibrosis.

MMTV-Spy1 male mice show increased incidence of HCC, fat accumulation, mediators of the DDR and proliferation. This occurs coincident with a decrease in fibrotic markers. This presents the intriguing hypothesis that Spy1 may be a driver of NAFLD-HCC without fibrosis, and is naturally downregulated during the progression to fibrosis/cirrhosis to allow for deposition of fibrotic material in the chronically injured liver. To test this hypothesis, wildtype B6CBAF1/J mice were given the methionine-choline deficient (MCD) or an amino acid control diet. The MCD diet is a commonly used diet to induce NASH in a well characterized manner (47). Beginning at 8 to 12 weeks of age, wild type mice were put on the MCD or amino acid control diet and time points were collected throughout ranging from 2 days to 6 weeks (Figure 4A), to determine the endogenous regulation of Spy1 as compared to markers indicative of stress/proliferation (fat increase), inflammation (TNFa) and fibrosis (trichrome staining). As expected, there was a significant increase in fat accumulation as assessed by Oil Red O staining by day 3, persisting for 7 days (Figure 4B). Fibrosis and TNFa were detectable 6 weeks post-treatment (Figures 4C-E). Spy1 levels were elevated during the early stages of disease when the

initial injury response would occur and fat would accumulate, being most pronounced at day 3 and declining from 1-4 weeks to baseline levels, prior to detection of fibrosis or the increase in inflammatory signaling (Figure 4D). Taken together this data suggests, that endogenous Spy1 is upregulated during the initial stress response and downregulated as the liver progresses towards fibrosis.

Elevated levels of Spy1 inhibit fibrosis.

Spy1 levels are naturally downregulated during the progression to fibrosis. This presents the additional hypothesis that aberrant elevation of levels of Spy1 may trigger the onset of HCC before progression to fibrosis/cirrhosis can occur. To test this, aged MMTV-Spy1 mice were placed on the MCD diet for 6 weeks and levels of proliferation and fibrosis were quantified (Figure 5A). MMTV-Spy1 mice had a decrease in liver to body weight ratio as compared to littermate controls (Figure 5B). The amount of fat accumulation in MMTV-Spy1 as compared to littermate controls was not significantly different after 6 weeks on the MCD diet (Figure 5C). Fibrosis however, was significantly decreased in the MMTV-Spy1 mice (Figure 5D). While there was no significant difference in TNFa between control and MMTV-Spy1 mice on the MCD diet, there was a significant increase in TNFa in mice on the MCD diet as compared to mice on a control diet (Figure S6A). PCNA staining further confirms that the MMTV-Spy1 mice have a significant increase in proliferation over control littermates (Figure 5E). Additionally, there were no changes to either the Kupffer or stellate cell population as assessed via expression of F4/80 and α-smooth muscle actin respectively (Figure S6B-C). It is notable that two MMTV-Spy1 mice on the MCD diet developed liver tumours while none of the control mice had any evidence of HCC upon completion of the diet. Thus, elevation of Spy1 appears to decrease the deposition of fibrotic material and increase rates of proliferation in the face of liver stressors.

Spy1 enhances tumourigenic properties and resistance to treatment.

To determine if elevated Spy1 alters classic tumorigenic properties in liver cells, Spy1 overexpression and knockdown was performed in HepG2 cells and a soft agar colony formation

assay was used to assess cellular transformation. Spy1 overexpression significantly increased the number of colonies formed, while knockdown of Spy1 showed no difference as compared to control (Figure 6A). To assess the therapeutic implications of alterations in Spy1 levels, HepG2 cells were treated with the CDK inhibitor, Roscovitine, or the multi-kinase inhibitor, Sorafenib in the presence or absence of Spy1. In both cases, knockdown of Spy1 resulted in increased sensitivity to treatment while overexpression of Spy1 resulted in enhanced resistance to treatment (Figure 6B). To further validate the effects of Spy1 manipulation on tumour growth, HepG2 cells with Spy1 overexpression or knockdown were subcutaneously injected into Nu/Nu mice, and rates of tumour growth were monitored (Figure 6C). Spy1 overexpression significantly increased tumour volume as compared to control tumours, while the knockdown of Spy1 lead to a significant reduction in tumour volume. Thus, elevated levels of Spy1 enhances tumourigenic capabilities and increases resistance to treatment *in vitro*.

Elevated expression of the SPDYA gene is associated with non-cirrhotic HCC.

We assessed the expression of *SPDYA* in normal tissue versus HCC using publicly available databases (Figures 6D & S7-10). In alignment with a previously published report (32), when compared to normal tissue, HCC has higher expression of *SPDYA* (Figure S7A). *SPDYA* expression increases with HCC grade and stage through to stage 3, with expression plateauing in stage 4 disease (Figure S7B-C). *SPDYA* levels were not different between normal weight and obese patients (Figure S7D), nor were there differences between male or female HCC patients (Figure S7E). Importantly, patients with higher expression levels of Spy1 have a lower survival probability, demonstrating that *SPDYA* expression correlates with poor prognosis (Figure S7F). Next we clustered the TCGA data based on *SPDYA* expression levels (Figure S8). Levels of Spy1 were not significantly different when samples were clustered based on Ishak Score (Figure S8C), however when cirrhotic HCC was assessed in Spy1 low and high groupings (Figure S8D), we found that the incidence of cirrhotic HCC is proportional with the level of Spy1 (Figure 6D). The expression of additional cell cycle mediators across fibrosis stage was assessed to determine if

this finding was unique to Spy1. While low *SPDYA* expression is associated with cirrhosis, expression of other cell cycle regulators, such as CDK2 and E2F1, was upregulated with cirrhosis (Figure S9).

Gene expression analysis was performed between Spy1 low and high groups to validate findings from the MMTV-Spy1 mouse. Higher expression of genes associated with lipid clearance, fatty acid oxidation and catabolism and lipid homeostasis were found in samples with low levels of Spy1 (Figure S10), while higher expression of genes associated with positive cell cycle regulation, regulation of CDKs, and suppression of genes which regulate the cellular response to DNA damage and DNA recombination were found in samples with high levels of Spy1 (Figure S11). Thus, elevated levels of Spy1 are associated with poor survival, the presence of non-cirrhotic HCC and expression of genes associated with enhanced cell cycle regulation and a decreased DDR.

Overall, our data presents the first characterization of a novel mouse model where Spy1 levels are elevated in male livers and promote susceptibility to HCC. Increased protein levels of Spy1 drives *in vivo* and *in vitro* proliferation of liver cells. This occurs at the expense of protective apoptotic or fibrotic programs in the damaged liver *in vivo*. This supports a model where cell cycle checkpoints carefully balance regeneration versus protective apoptotic/fibrotic programs and enhanced proliferation promotes HCC prior to disease progression (Figure 6E).

Discussion

The MMTV-Spy1 transgenic mouse model was initially generated to study the effects of aberrant Spy1 expression on mammary gland development and tumourigenesis. The MMTV promoter is well documented and has been shown to induce expression of the transgene in various tissue types with the most common organs affected being secretory organs such as the salivary gland (48). There have been however, documented cases of transgene expression in the liver (37). We were surprised to find a significant increase in rates of liver tumour formation uniquely in male MMTV-Spy1 mice. Importantly, these were single large masses consistent with what is seen in

non-cirrhotic HCC, as opposed to the multi-focal nature of cirrhotic-HCC (49). Indeed, increased levels of Spy1 were found in aged MMTV-Spy1 male livers and transgene expression was not noted in livers of aged females. Sexual dichotomy in MMTV transgene expression has been found in other male tissues, such as male reproductive organs (50). Androgen responsive elements have been noted within the MMTV promoter thus indicating the possibility that androgen stimulation could lead to male specific liver expression of the transgene (50). Our data is hence only able to address liver tumour initiation in male livers due to the expression pattern driven by the transgene utilized.

Histological analysis revealed key differences in MMTV-Spy1 and control liver tissue. Livers of MMTV-Spy1 mice displayed increased levels of fat. Accompanying this, was a significant decrease in levels of genes associated with lipid catabolism, and no changes with genes involved in de novo lipogenesis. This suggests that livers of the MMTV-Spy1 mice are unable to properly break down fat deposition leading to increases in fat deposits within the liver. This manifestation could have profound consequences on the development of HCC and play a key role in its progression. Fatty acids trigger an inflammatory response, leading to increased injury to the liver that hepatocytes would typically be able to repair (6,10). In cases of severe injury, hepatocytes ultimately senesce or undergo apoptosis diminishing the ability of the liver to repair injured areas of tissue (6). Elevated levels of p53 are found in cases of NASH and positively correlate with increasing degrees of inflammation (13-15). Activation of p53 triggers up-regulation of its downstream target p21, which arrests the cell cycle, and ultimately, p53 will lead to apoptosis of damaged hepatocytes (13,15). MMTV-Spy1 mice display characteristics of a severely diseased liver. We see increased levels of p53 and p21 indicating significant injury or damage and inflammation. Additionally, a key mediator of the inflammatory response, TNFa, was also significantly decreased in MMTV-Spy1 mice. Since Spy1 is capable of promoting cell cycle progression, it is plausible that increased amounts of Spy1 could in fact be triggering elevated rates of DNA replication leading to increased rates of proliferation and a decrease in bi-

nucleated cells. Indeed, we see a significant decrease in the number of bi-nucleated cells and ploidy in MMTV-Spy1 mice which may be indicative of enhanced proliferation. This finding was validated through BrdU incorporation assays where MMTV-Spy1 mice showed enhanced rates of proliferation. Bi-nucleation and enhanced proliferation may be indicative of decreased ploidy which has been shown to play a role in accelerating tumourigenesis (25). While the change in ploidy is small, this may have significant consequences on disease susceptibility. Expression of various cell cycle mediators were assessed and levels of C/EBPa were found to be significantly decreased. C/EBPa is an important inhibitor of cell cycle progression in hepatocytes, holding the cells in quiescence (46). The mechanism by which Spy1 decreases levels of C/EBPa warrants further investigation as this may reveal novel insight of mechanisms of not only initiation of HCC, but also defects in liver regeneration. Taken together, these data support the hypothesis that Spy1 enhances proliferation in the face of damage which may lead to increased susceptibility to tumourigenesis preventing liver disease progression.

To study the role of endogenous Spy1 during the progression of NASH we induce NASH in a mouse model using the MCD diet. Data demonstrates that in wild-type mice endogenous Spy1 levels are significantly elevated in the early stages of disease progression and are significantly downregulated as inflammatory response pathways are activated and the liver becomes primed for fibrosis. When MMTV-Spy1 mice are placed on the MCD diet they had significantly less fibrotic material in their livers than their control littermates. Thus, this data demonstrates for the first time that a gene linked to elevated HCC can override protective fibrotic responses in the liver and promote enhanced proliferation.

In humans Spy1 levels are elevated in HCC when compared to pair matched normal tissue and Spy1 levels correlated with proliferation index of patient tumours, increasing severity of disease and poor prognosis (32). Our data combined with these clinical observations supports that the mechanism of Spy1-induced proliferation is worthy of further research and may elute attractive therapeutic targets in treatment of devastating liver diseases.

Abbreviations

CDK: Cyclin-dependent kinase; DDR: DNA damage response; HCC: Hepatocellular Carcinoma; MCD: methionine choline deficient; NALFD: non-alcoholic fatty liver disease; NASH: non-alcoholic steatohepatitis

Declarations

Ethics Approval

All experiments performed were approved by the University of Windsor Animal Care Committee.

Competing Interests

The authors have no competing interests to declare.

Funding

This work was supported by Canadian Institutes Health Research to L.A.P (Grant#142189) and the Windsor Cancer Centre Foundation's Seeds4Hope Program. B.F. acknowledges support from the University of Windsor, the Ontario Graduate Scholarship Program and Canadian Breast Cancer Foundation.

Availability of Data and Materials

All data generated from this study are included in the manuscript and additional file 1 supplemental files.

Authors Contributions

LAP and BF designed experiments and wrote the manuscript. BF, JT, CS, ME, MKB, AB, JPS, MC and KFS performed experiments and data analysis. All authors approved the final manuscript.

Consent for Publication

All authors have agreed to publish this manuscript.

Acknowledgements

We thank Dr. Christopher Pin and Linsay Drysdale from the London Regional Transgenic and

Gene Targeting Facility for generation of the MMTV-Spy1 mouse, and the Mutant Mouse Pathology Lab, Center for Comparative Medicine, University of California, Davis and Dr. Robert Cardiff for additional pathology support. Thanks to Dr. John Hudson for donation of HepG2 cells, and Dr. Dennis Higgs for use of equipment. Special thanks to Dr. Dorota Lubanska, Dr. Ingrid Qemo, Ellen Laurie and Nick Paquette for assistance with genotyping. Portions of this manuscript cross check with BF dissertation which is available publicly online.

Supporting Information

S1 Figure. Female liver analysis in MMTV-Spy1 mice.

S2 Figure. Alterations in levels of Spy1 in HCC cell lines lead to changes in lipid content.

S3 Figure. Spy1 elevation leads to changes in lipid catabolism.

S4 Figure. Marker analysis supports that Spy1 bypasses functional checkpoints in the liver.

S5 Figure. Spy1 drives proliferation in human HCC and alters C/EBPa.

S6 Figure. Spy1 does not alter inflammation or non-parenchymal cell populations during fibrosis.

S7 Figure. Higher Expression of SPDYA is associated with poor outcomes

S8 Figure. Classification of HCC samples based on Spy1 expression.

S9 Figure. The expression pattern of cell cycle regulators in HCC samples with different Ishak fibrosis stage.

S10 Figure. *SPDYA* expression correlates with lower expression of lipid metabolism genes.

S11 Figure. High expression of *SPDYA* correlates with increased expression of positive cell cycle regulators.

S1 Supplemental Materials and Methods. Additional Materials and Methods.

S2 Supplemental Figure Legends. Figure legends for supplemental figures.

References

1. World Health Organization. (2014) Cancer. http://www.who.int/mediacentre/factsheets/fs297/en/.
2. Fattovich, G., *et al.* (2004) Hepatocellular carcinoma in cirrhosis: incidence and risk factors. *Gastroenterology*, **127**, S35-50.
3. Liu, Y., *et al.* (2010) Global burden of aflatoxin-induced hepatocellular carcinoma: a risk assessment. *Environ Health Perspect*, **118**, 818-24.
4. Koh, W.P., *et al.* (2013) Diabetes mellitus and risk of hepatocellular carcinoma: findings from the Singapore Chinese Health Study. *Br J Cancer*, **108**, 1182-8.
5. Bataller, R., *et al.* (2005) Liver fibrosis. *J Clin Invest*, **115**, 209-18.
6. Dowman, J.K., *et al.* (2010) Pathogenesis of non-alcoholic fatty liver disease. *QJM*, **103**, 71-83.
7. Schutte, K., *et al.* (2014) Characterization and prognosis of patients with hepatocellular carcinoma (HCC) in the non-cirrhotic liver. *BMC Gastroenterol*, **14**, 117.
8. Adams, L.A., *et al.* (2005) Nonalcoholic fatty liver disease. *Canadian Medical Association Journal*, **172**, 899-905.
9. Ertle, J., *et al.* (2011) Non-alcoholic fatty liver disease progresses to hepatocellular carcinoma in the absence of apparent cirrhosis. *Int J Cancer*, **128**, 2436-43.
10. Jou, J., *et al.* (2008) Mechanisms of disease progression in nonalcoholic fatty liver disease. *Semin Liver Dis*, **28**, 370-9.
11. Sancar, A., *et al.* (2004) Molecular mechanisms of mammalian DNA repair and the DNA damage checkpoints. *Annu Rev Biochem*, **73**, 39-85.
12. Meek, D.W. (2004) The p53 response to DNA damage. *DNA Repair (Amst)*, **3**, 1049-56.
13. Farrell, G.C., *et al.* (2009) Apoptosis in experimental NASH is associated with p53 activation and TRAIL receptor expression. *J Gastroenterol Hepatol*, **24**, 443-52.
14. Panasiuk, A., *et al.* (2006) Expression of p53, Bax and Bcl-2 proteins in hepatocytes in non-alcoholic fatty liver disease. *World J Gastroenterol*, **12**, 6198-202.
15. Yahagi, N., *et al.* (2004) p53 involvement in the pathogenesis of fatty liver disease. *J Biol Chem*, **279**, 20571-5.
16. Derdak, Z., *et al.* (2013) Inhibition of p53 attenuates steatosis and liver injury in a mouse model of non-alcoholic fatty liver disease. *J Hepatol*, **58**, 785-91.
17. Ehrenfried, J.A., *et al.* (1997) Cell cycle-mediated regulation of hepatic regeneration. *Surgery*, **122**, 927-35.
18. Fausto, N., *et al.* (2003) The role of hepatocytes and oval cells in liver regeneration and repopulation. *Mech Dev*, **120**, 117-30.
19. Webber, E.M., *et al.* (1994) In vivo response of hepatocytes to growth factors requires an initial priming stimulus. *Hepatology*, **19**, 489-97.
20. Bisteau, X., *et al.* (2014) The Complex Relationship between Liver Cancer and the Cell Cycle: A Story of Multiple Regulations. *Cancers (Basel)*, **6**, 79-111.
21. Michalopoulos, G.K. (2007) Liver regeneration. *J Cell Physiol*, **213**, 286-300.
22. Zou, Y., *et al.* (2012) Four waves of hepatocyte proliferation linked with three waves of hepatic fat accumulation during partial hepatectomy-induced liver regeneration. *PLoS One*, **7**, e30675.
23. Menendez, J.A., *et al.* (2007) Fatty acid synthase and the lipogenic phenotype in cancer pathogenesis. *Nat Rev Cancer*, **7**, 763-77.
24. Alkhouri, N., *et al.* (2011) Apoptosis in nonalcoholic fatty liver disease: diagnostic and therapeutic implications. *Expert Rev Gastroenterol Hepatol*, **5**, 201-12.

25. Zhang, S., *et al.* (2018) The Polyploid State Plays a Tumor-Suppressive Role in the Liver. *Dev Cell*, **44**, 447-459 e5.
26. Cheng, A., *et al.* (2005) Biochemical characterization of Cdk2-Speedy/Ringo A2. *BMC Biochem*, **6**, 19.
27. Porter, L.A., *et al.* (2002) Human Speedy: a novel cell cycle regulator that enhances proliferation through activation of Cdk2. *J Cell Biol*, **157**, 357-66.
28. Lenormand, J.L., *et al.* (1999) Speedy: a novel cell cycle regulator of the G2/M transition. *Embo J*, **18**, 1869-77.
29. McGrath, D.A., *et al.* (2017) Structural basis of divergent cyclin-dependent kinase activation by Spy1/RINGO proteins. *EMBO J*, **36**, 2251-2262.
30. McAndrew, C.W., *et al.* (2009) The atypical CDK activator Spy1 regulates the intrinsic DNA damage response and is dependent upon p53 to inhibit apoptosis. *Cell Cycle*, **8**, 66-75.
31. Gastwirt, R.F., *et al.* (2006) Spy1 expression prevents normal cellular responses to DNA damage: inhibition of apoptosis and checkpoint activation. *J Biol Chem*, **281**, 35425-35.
32. Ke, Q., *et al.* (2009) Expression and prognostic role of Spy1 as a novel cell cycle protein in hepatocellular carcinoma. *Exp Mol Pathol*, **87**, 167-72.
33. Fifield, B.-A., *et al.* (2019) The Atypical Cyclin-Like Protein Spy1 Overrides p53-Mediated Tumour Suppression and Promotes Susceptibility to Breast Tumorigenesis. *bioXriv*.
34. Lubanska, D., *et al.* (2014) The cyclin-like protein Spy1 regulates growth and division characteristics of the CD133+ population in human glioma. *Cancer Cell*, **25**, 64-76.
35. Vargo-Gogola, T., *et al.* (2006) P190-B Rho GTPase-activating protein overexpression disrupts ductal morphogenesis and induces hyperplastic lesions in the developing mammary gland. *Mol Endocrinol*, **20**, 1391-405.
36. Bojic, L.A., *et al.* (2014) PPARdelta activation attenuates hepatic steatosis in Ldlr-/- mice by enhanced fat oxidation, reduced lipogenesis, and improved insulin sensitivity. *J Lipid Res*, **55**, 1254-66.
37. Wagner, K.U., *et al.* (2001) Spatial and temporal expression of the Cre gene under the control of the MMTV-LTR in different lines of transgenic mice. *Transgenic Res*, **10**, 545-53.
38. Wang, X., *et al.* (1998) Relationship between tumor necrosis factor-alphaand liver fibrosis. *World J Gastroenterol*, **4**, 18.
39. Gabele, E., *et al.* (2009) TNFalpha is required for cholestasis-induced liver fibrosis in the mouse. *Biochem Biophys Res Commun*, **378**, 348-53.
40. Mogler, C., *et al.* (2015) Hepatic stellate cell-expressed endosialin balances fibrogenesis and hepatocyte proliferation during liver damage. *EMBO Mol Med*, **7**, 332-8.
41. Bilzer, M., *et al.* (2006) Role of Kupffer cells in host defense and liver disease. *Liver Int*, **26**, 1175-86.
42. Li, J.T., *et al.* (2008) Molecular mechanism of hepatic stellate cell activation and antifibrotic therapeutic strategies. *J Gastroenterol*, **43**, 419-28.
43. Kolios, G., *et al.* (2006) Role of Kupffer cells in the pathogenesis of liver disease. *World J Gastroenterol*, **12**, 7413-20.
44. Gentric, G., *et al.* (2012) Hepatocytes polyploidization and cell cycle control in liver physiopathology. *Int J Hepatol*, **2012**, 282430.
45. Jack, E.M., *et al.* (1990) Increase in hepatocyte and nuclear volume and decrease in the population of binucleated cells in preneoplastic foci of rat liver: a stereological study using the nucleator method. *Hepatology*, **11**, 286-97.

46. Timchenko, N.A., *et al.* (1997) CCAAT/enhancer binding protein alpha regulates p21 protein and hepatocyte proliferation in newborn mice. *Mol Cell Biol*, **17**, 7353-61.
47. Machado, M.V., *et al.* (2015) Mouse models of diet-induced nonalcoholic steatohepatitis reproduce the heterogeneity of the human disease. *PLoS One*, **10**, e0127991.
48. Cardiff, R.D., *et al.* (2011) A compendium of the mouse mammary tumor biologist: from the initial observations in the house mouse to the development of genetically engineered mice. *Cold Spring Harb Perspect Biol*, **3**.
49. Smalley, S.R., *et al.* (1988) Hepatoma in the noncirrhotic liver. *Cancer*, **62**, 1414-24.
50. Parker, M.G., *et al.* (1987) Identification of androgen response elements in mouse mammary tumour virus and the rat prostate C3 gene. *J Cell Biochem*, **35**, 285-92.

Figure Legends

Figure 1: MMTV-Spy1 male mice are more susceptible to liver tumourigenesis. A) Graphical representation of percentage of mice with liver tumourigenesis (MMTV-Spy1 n=23, Cntl n=23). B) qRT-PCR analysis of MMTV-Spy1 and littermate control liver samples for Spy1 levels in males (MMTV-Spy1 n=14, Cntl n=10) corrected for total GAPDH levels. C) Representative H&E stain of liver tissue collected from male mice over the age of 1 year. Scale bar= 50 uM. D) Oil-Red-O staining was performed on MMTV-Spy1 mice and control littermates to assess fat content within the livers. Staining was quantified using ImageJ and corrected for area (top panel). Representative images shown on the bottom panel (Cntl n=10, MMTV-Spy1 n=9) Scale bar=100μM. E) Hepatic triglyceride content normalized to wet tissue weight in control or MMTV-Spy1 mice (Cntl n=8 MMTV-Spy1 n=6). Error bars reflect SE, Mann-Whitney (A) and Student's T-test (B, D, E) *$p<0.05$, ***$p<0.001$

Figure 2: MMTV-Spy1 mice show enhanced DNA damage signaling and decreased inflammation and fibrosis. Immunohistochemical analysis of MMTV-Spy1 or littermate controls (cntl). Male livers were analysed over a minimum of 4 fields of view per sample and levels were quantified using ImageJ analysis software correcting for number of cells present per field of view. Representative images are shown in left panels, and quantification of expression is depicted in right panels. Blue stain is haematoxylin and brown stain is primary antibody. A) Analysis of p53 levels (MMTV-Spy1 n=5, Cntl n=4). B) Analysis of p21 levels (MMTV-Spy1 n=5, Cntl n=4). C) Analysis of cleaved caspase 3 (MMTV-Spy1 n=4, Cntl n=3) D) Levels of TNFa were assessed via qRT-PCR and were corrected for total GAPDH (Cntl n=26, MMTV-Spy1 n=27). E) Masson's trichrome staining was performed to stain for fibrotic tissue with representative images shown in the bottom panel. Images were quantified using ImageJ software to assess the area stained for fibrotic tissue. Quantification is shown in the top panel. F) Immunohistochemical analysis of F4/80 to assess the Kupffer cell population (lower panel). Percent area stained was quantified

using ImageJ software (upper panel) (n=5). Error bars reflect SE; Students T-test *p<0.05, **p<0.01, ***p<0.001. Scale bar=0.1 mm.

Figure 3: MMTV-Spy1 mice have increased proliferation. A) Number of binucleated cells was counted in MMTV-Spy1 mice and their control littermates. Percentage of binucleated cells is depicted graphically (MMTV-Spy1 n=16, Cntl n=16). B) Primary hepatocytes from MMTV-Spy1 mice and control littermates were assessed for DNA content via flow cytometry (n=3). C) BrdU incorporation was assessed in MMTV-Spy1 mice and their control littermates with representative images shown in the right panel. The percentage of BrdU positive cells were quantified and are shown in the left panel. Scale bar= 100μM. D) The percent cells positive for PCNA was quantified as shown in the left panel. Representative images are shown in the right panel (MMTV-Spy1 n=7, Cntl n=8). Scale bar=100μM. Scale bar= 50 uM. Error bars reflect SE; Student's T-test *p<0.05, **p<0.01, ***p<0.001

Figure 4: Spy1 expression is downregulated during progression of NASH. A) Wildtype mice were placed on the MCD diet for 6 weeks and time points were collected throughout B) Oil Red staining was performed on wild-type mice fed both the MCD diet and amino acid control diet to assess fat content during disease progress. Stain intensity was measured and quantified using Image J analysis software (Cntl n=3 MCD n=3). C) Trichome staining was performed on MCD and amino acid control diet mice 6 weeks after being placed on the diet to assess the onset of fibrosis (Cntl n=3 MCD n=3). Representative images of a control mouse (left panel) and an MCD mouse (right panel) is shown. Western blot analysis was performed to assess the levels of D) Spy1 (Day 2 Cntl n=10 MCD n= 13; Day 3 MCD n= 5; 1 week MCD n=10; 4 week MCD n=4; 6 week MCD n=12) during the diet time course. Levels of Spy1 were measured and corrected for Actin with densitometry analysis. E) qRT-PCR analysis of TNFa expression in amino acid control and MCD diet mice corrected for total GAPDH levels (Day 2 Cntl n=5, MCD n=6; Day 3

MCD n=7; 1 week MCD n=7; 4 week MCD n=6; 6 week MCD n=7). Error bars reflect SE; Students T-test *p<0.05, **p<0.01

Figure 5: Elevated levels of Spy1 inhibit the onset of fibrosis. A) MMTV-Spy1 aged male mice were placed on the MCD diet for 6 weeks. B) Liver to body weight ratio was measured for MMTV-Spy1 and control littermates after the 6 week treatment (Cntl n=6, MMTV-Spy1 n=10) C) Oil Red analysis was performed on MMTV-Spy1 mice and their control littermates on the MCD diet to assess amount of fat present in the liver. Staining intensity was measured and quantified using Image J analysis software. (Cntl n=6, MMTV-Spy1 n=10). D) The onset of fibrosis was analysed via a Masson's Trichrome stain which was quantified using Image J analysis software to determine the percentage of area stained. Representative images are shown in the right panel and quantification is shown on the left panel. Scale bar= 100µM (Cntl n= 5, MMTV-Spy1 n=5). E) Immunohistochemical analysis for percent positive PCNA staining with representative images on the right and quantification on the left. Scale bar= 100µM (Cntl n= 6, MMTV-Spy1 n=9). Error bars reflect SE; Students T-test *p<0.05, **p<0.01, ***p<0.001.

Figure 6: Spy1 levels dictate tumourigenic potential. A) HepG2 cells were transfected with pEIZ, pEIZ-Spy1, pLKO or pLKO-shSpy1 and seeded in soft agar for colony formation. Total number of colonies was quantified (n=3). B) HepG2 cells were transfected with pEIZ, pEIZ-Spy1, pLKO or pLKO-shSpy1 and treated with 10µM Roscovitine or 5µM Sorafenib. Cell survival was assessed via the trypan blue exclusion assays 24 hours post treatment (n=3). C) HepG2 cells transfected with pEIZ, pEIZ-Spy1, pLKO or pLKO-shSpy1 were injected subcutaneously in Nu/Nu mice and tumour volume was measured twice per week. Fold change in tumour volume with Spy1 overexpression (n=10) and Spy1 knockdown (n=10) is depicted graphically. D) The prevalence of non-cirrhotic and cirrhotic HCC in SPDYA low, and high cases of HCC. E) Liver disease progression. Risk factors for HCC include NAFLD and fibrosis/cirrhosis. It is known that

a subset of patients can develop HCC without indicators of fibrosis. Our data supports that Spy1 promotes the development of NAFLD-HCC without fibrosis through increased proliferation and bypassing cellular checkpoints. Error bars reflect SE; Students T-test *p<0.05, **p<0.01, ***p<0.001

Figure 1

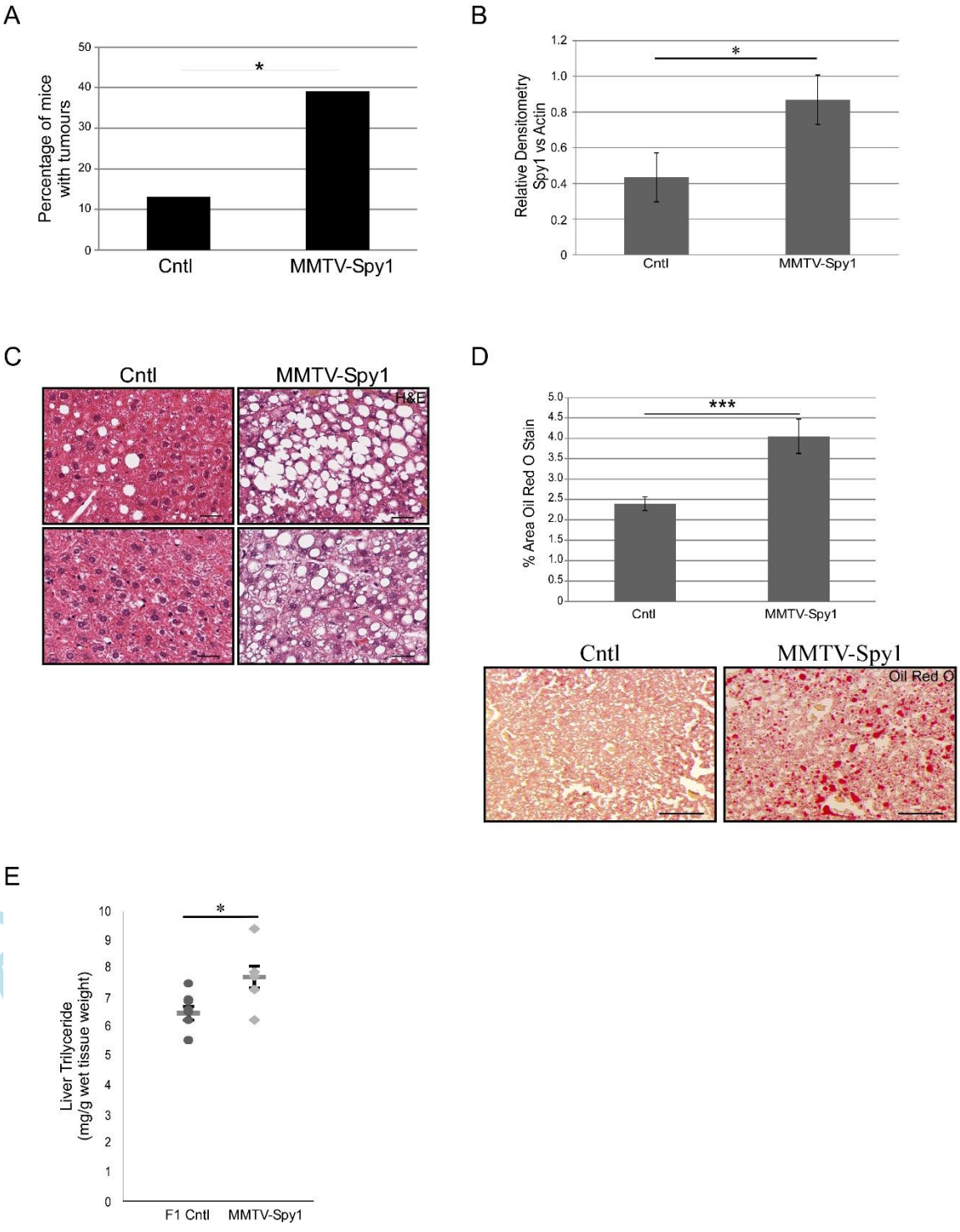

Figure 2

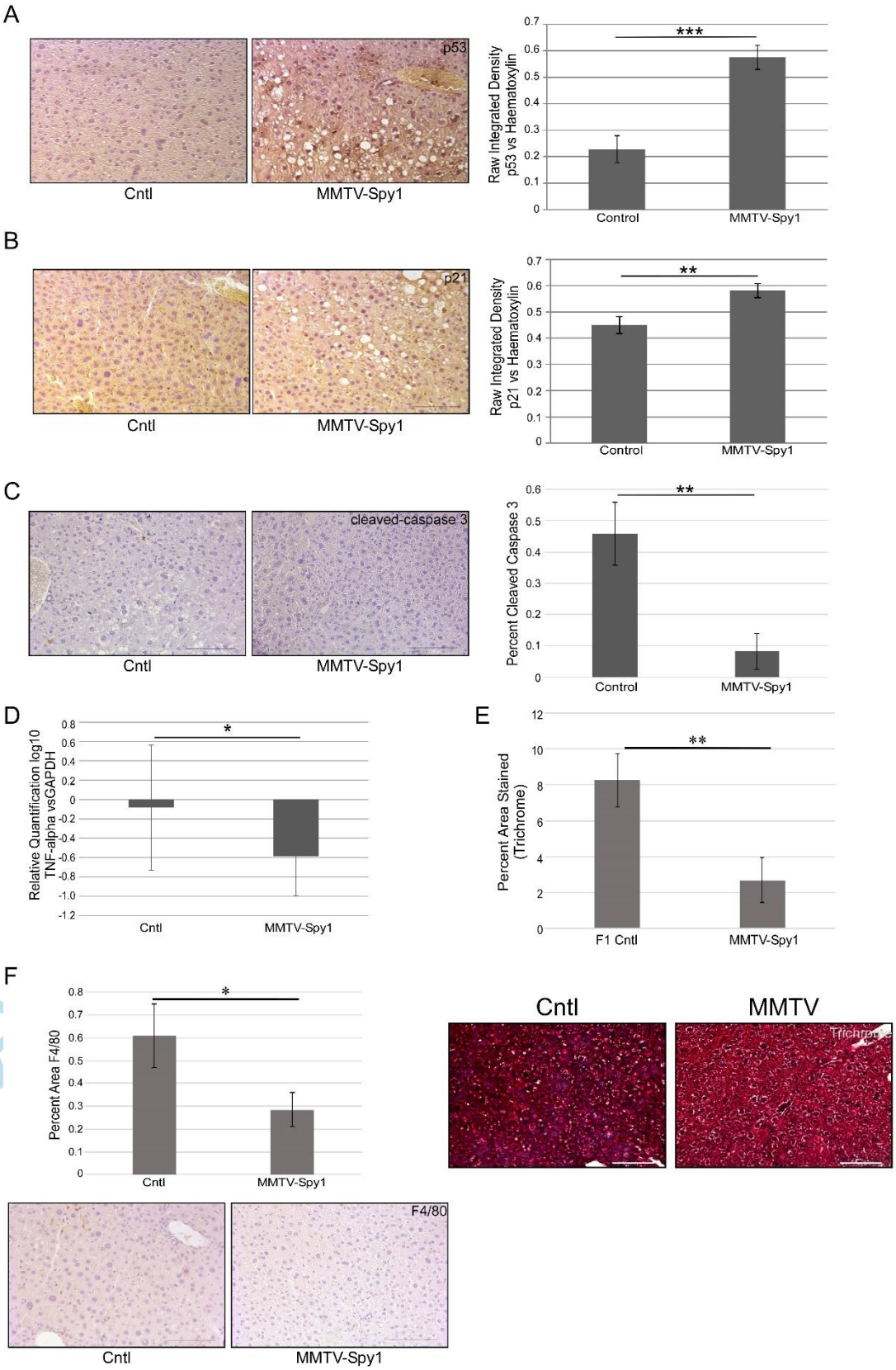

Figure 3

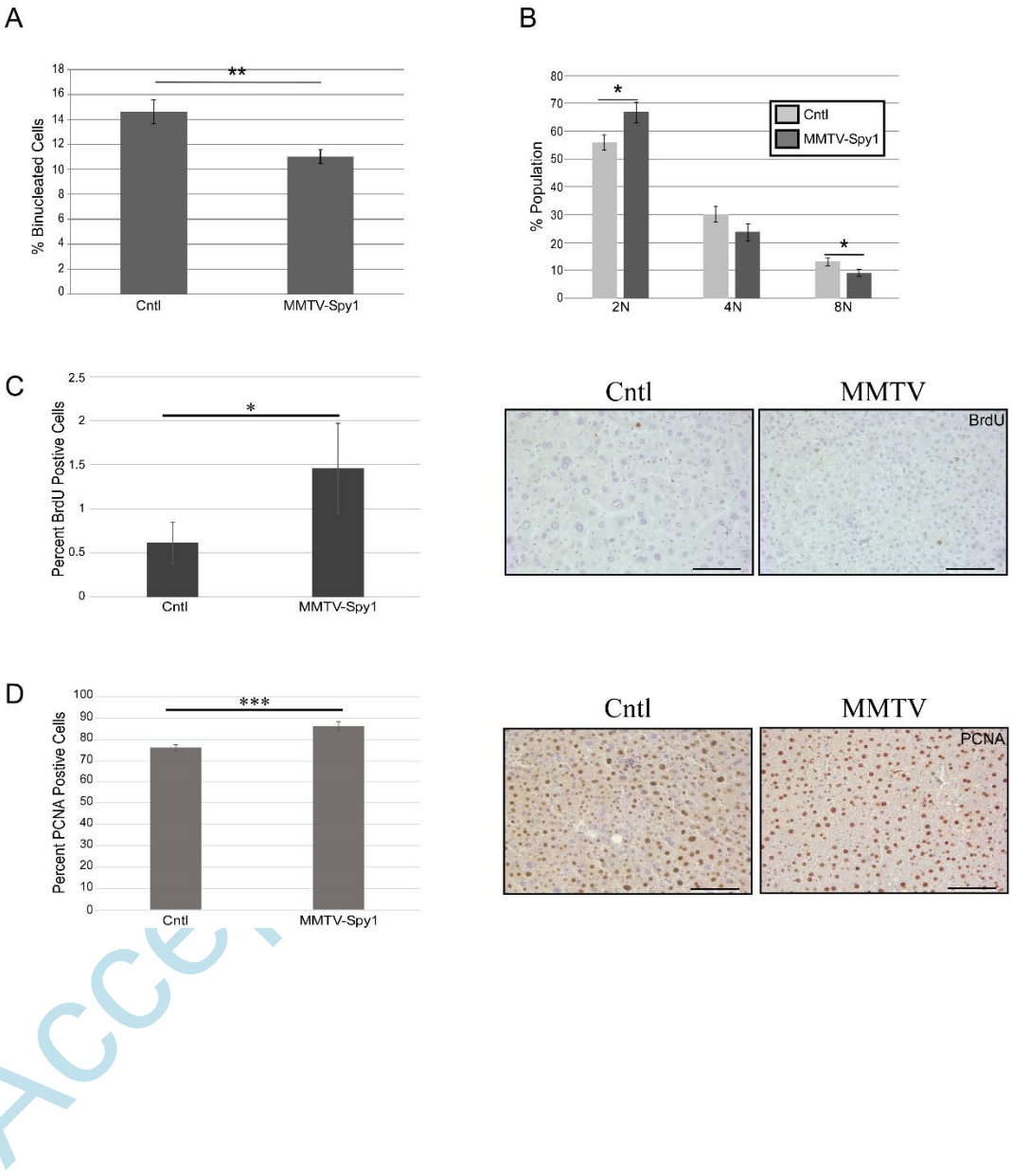

Figure 4

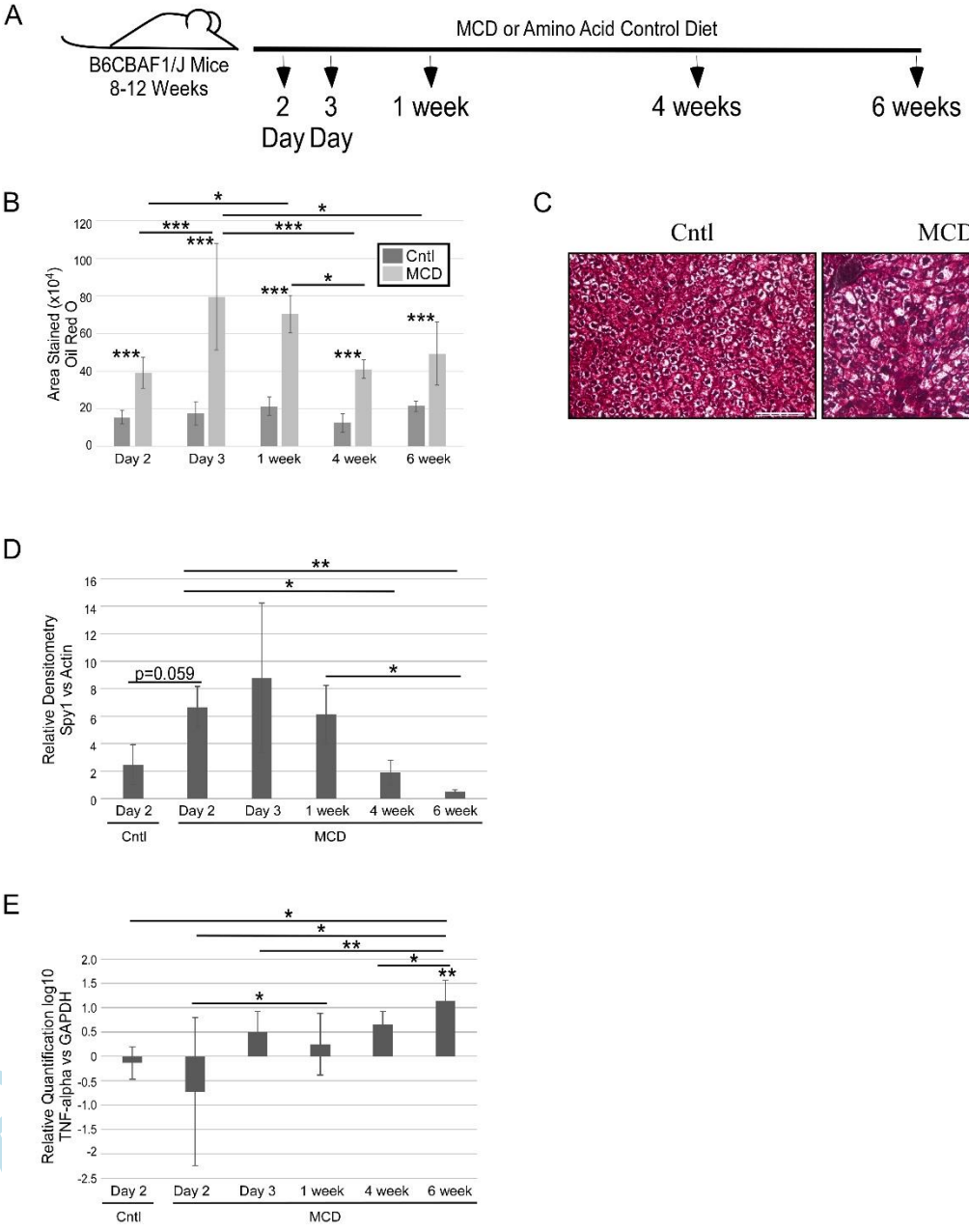

Figure 5

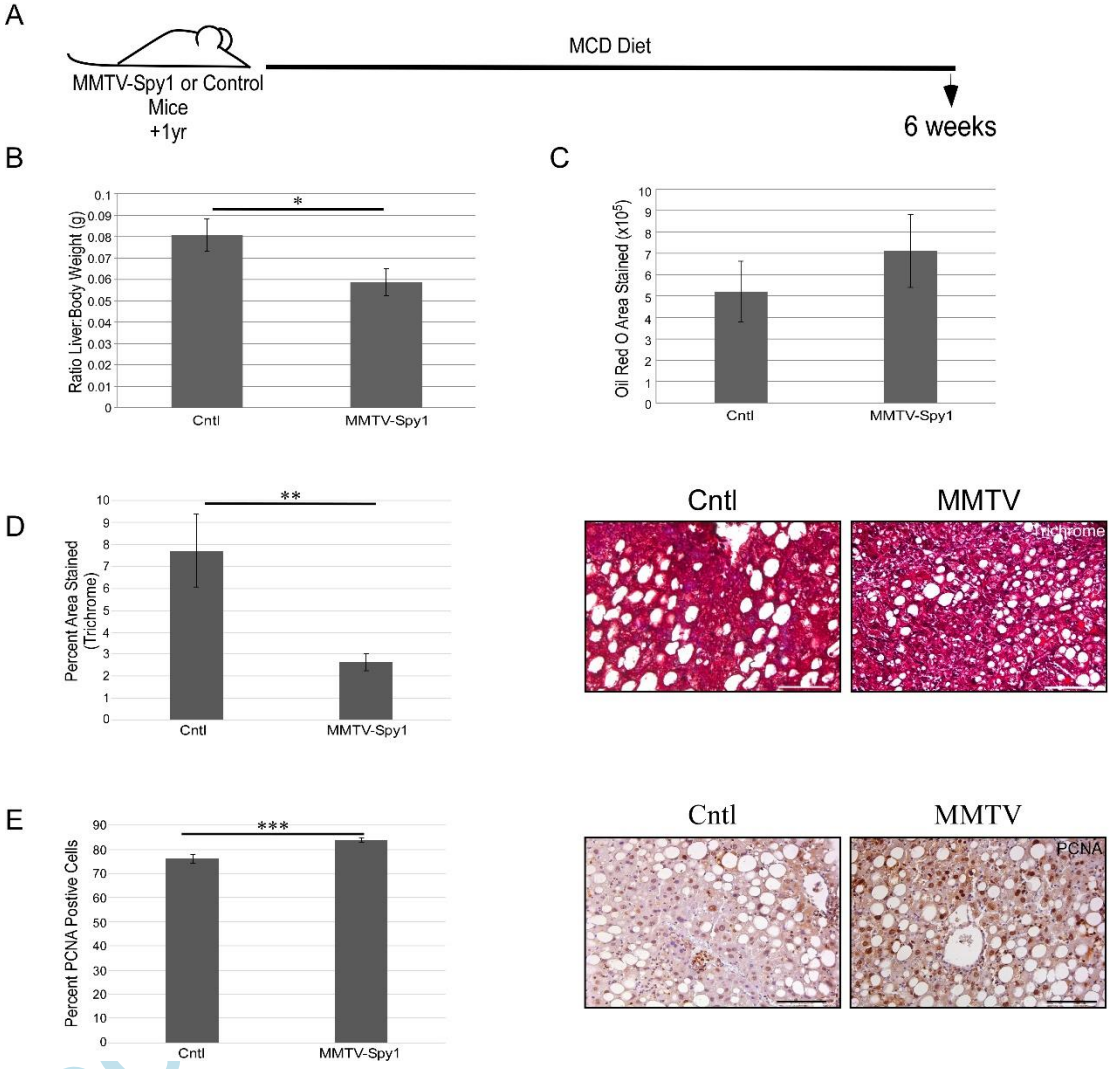

Figure 6